Inhibition of atomic phase decays by squeezed light in a microscopic Fabry-Pérot cavity

A. S. Parkins and C. W. Gardiner
Physics Department, University of Waikato, Hamilton, New Zealand
(Received 14 November 1988; revised manuscript received 28 March 1989)

The inhibition of atomic phase decays by squeezed light, as first predicted by Gardiner [Phys. Rev. Lett. **56**, 1917 (1986)], has yet to be confirmed experimentally. A major obstacle to such an experiment is the production of an effective squeezed-vacuum–atom coupling, so that the atom interacts only with squeezed modes of the radiation field. In this paper we propose the use of a microscopic plane-mirror Fabry-Pérot cavity to effect a strong selection of modes coupling to the atom. It is shown that a significant reduction in fluctuations experienced by the atom can be achieved in one quadrature, with an input squeezed beam of modest angular dimensions, provided that the phase (and to lesser extent the amplitude) characteristics of the input beam are suitably matched to the cavity.

I. INTRODUCTION

In recent years a number of very interesting phenomena have been predicted with regard to the interaction of squeezed light with atomic systems. Gardiner[1] first pointed out that squeezed light incident upon a single two-level atom can in principle inhibit the phase decay of that atom, giving rise to line narrowing in the spectrum of fluorescent light. In particular, that component of the atomic polarization which is in phase with the low-noise quadrature phase experiences reduced fluctuations relative to the vacuum, and so decays slower than the other component, which experiences increased fluctuations.

Since that first paper, analyses have been extended to the treatment of resonance fluorescence[2] and atomic absorption spectra[3] in a squeezed vacuum, atomic level shifts in a squeezed vacuum,[4] squeezed pump lasers,[5] and most recently to photon echoes with coherent and squeezed pulses.[6]

Further work has also been done to incorporate the effect of finite-bandwidth squeezing on the inhibition of atomic phase decays.[7] These investigations have shown that the essential predictions of the broadband (white-noise) theories are correct, provided that the bandwidth of squeezing (in both quadratures) is reasonably large compared to the natural linewidth of the transition. If this is not the case, inhibition of the phase decay will not occur. In this work, of course, we shall assume the former.

All of the above analyses have assumed an ideal coupling between the atoms and the squeezed vacuum; that is, the atom interacts only with squeezed modes of the radiation field. This is a significant practical problem which Gardiner pointed out in his original paper, stating the need for either an incoming squeezed electric dipole wave, or an appropriate one-dimensional situation.

The first suggestion presents somewhat formidable practical problems in holding atoms still at the focus, and consequently in minimizing Doppler effects. We will therefore develop the second approach, using as experimental support the recent work of De Martini and coworkers[8] with microscopic plane-mirror cavities. In their experiments, De Martini *et al.* use two parallel plane mirrors, separated by a distance L of the order of the spontaneous-emission wavelength λ. With this microscopic Fabry-Pérot cavity, a strong selection of radiation modes coupling to atoms within the cavity is possible. In particular, for $L=\lambda/2$, atoms whose dipole moments are parallel to the mirrors couple strongly and exclusively (for a cavity of sufficiently high finesse) to the modes whose propagation vectors lie within a small solid angle about a line perpendicular to the mirror surfaces. It is by squeezing these modes that we shall aim to achieve an effective squeezed-vacuum–atom coupling. Such a scheme would also seem to suit the likely source of squeezed light, a degenerate parametric oscillator, which in present experiments produces a near-plane-wave output.

II. EQUATIONS OF MOTION

The Heisenberg equations of motion, combined with the commutation relations for the field and atomic operators, form the basis of our analysis of the coupled atom-field system. Following the general principles of the input-output formalism,[7,9] modified to three dimensions, we solve firstly for the field, and then substitute this result into the equations of motion for the atomic "spin" operators. For a two-state atom, in the electric dipole approximation, we find

$$\begin{aligned}\dot{\sigma}^{-}(t)&=-i\omega_a\sigma^{-}(t)-\frac{i}{2\hbar}\boldsymbol{\mu}_{21}\cdot[\mathbf{E}^{\perp}(\mathbf{h},t),\sigma_z(t)]_+ ,\\ \dot{\sigma}_z(t)&=-\frac{i}{\hbar}\boldsymbol{\mu}_{21}\cdot[\mathbf{E}^{\perp}(\mathbf{h},t),\sigma^{-}(t)-\sigma^{+}(t)]_+ ,\end{aligned} \tag{2.1}$$

where ω_a is the atomic transition frequency, and $\boldsymbol{\mu}_{21}$ is the transition dipole moment. The vector $\mathbf{h}$ gives the position of the atom.

Important to the derivation of these equations is the fact that the system (the atom) and the bath (the field) represent independent degrees of freedom, and hence that equal-time commutators of atomic operators with field

operators must be identically zero.

The field $\mathbf{E}^{\perp}(\mathbf{h},t)$ that appears in (2.1) can be divided into two distinct contributions: a source-free or input term, and a radiated field due to the atom. This leads us to write

$$\mathbf{E}^{\perp}(\mathbf{h},t)=\mathbf{E}^{\perp}_{\text{in}}(\mathbf{h},t)+\mathbf{\Gamma}(\mathbf{h},t)\ , \tag{2.2}$$

where

$$\mathbf{E}^{\perp}_{\text{in}}(\mathbf{h},t)=i\sum_{\mathbf{k},s}\left[\frac{\hbar\omega_k}{2}\right]^{1/2}a_{\mathbf{k}s}(t_0)e^{-i\omega_k(t-t_0)}\mathbf{f}_{\mathbf{k}s}(\mathbf{h}) +\text{H.c.}, \tag{2.3}$$

$$\mathbf{\Gamma}(\mathbf{h},t)=i\sum_{\mathbf{k},s}\frac{\omega_k}{2}[\boldsymbol{\mu}_{21}\cdot\mathbf{f}^{*}_{\mathbf{k}s}(\mathbf{h})]\mathbf{f}_{\mathbf{k}s}(\mathbf{h})\sigma^{-}(t) \times\int_0^{t-t_0}d\tau\, e^{-i(\omega_k-\omega_a)\tau}+\text{H.c.}\ , \tag{2.4}$$

with $\mathbf{f}_{\mathbf{k},s}(\mathbf{h})$ the appropriate mode functions, evaluated at the position of the atom, and s the polarization index ($s=1,2$). The result (2.4) is not exact, in that we have assumed the atom-field interaction to be weak, allowing us to make the approximation $\sigma^{-}(t-\tau)\simeq\sigma^{-}(t)e^{i\omega_a\tau}$. This is generally referred to as the adiabatic approximation, and corresponds to a bad cavity limit, which we shall be assuming in this paper.

Using the expressions (2.3), (2.4), Eq. (2.1) can be cast in the form

$$\dot{\sigma}^{-}(t)=-i\omega_a\sigma^{-}(t)-\frac{i}{2\hbar}\boldsymbol{\mu}_{21}\cdot[\mathbf{E}^{\perp}_{\text{in}}(\mathbf{h},t),\sigma_z(t)]_+\ , \tag{2.5}$$

$$\dot{\sigma}_z(t)=-\beta(\mathbf{h})-\frac{i}{\hbar}\boldsymbol{\mu}_{21}\cdot[\mathbf{E}^{\perp}_{\text{in}}(\mathbf{h},t),\sigma^{-}(t)-\sigma^{+}(t)]_+\ ,$$

where

$$\beta(\mathbf{h})=\frac{1}{2\hbar}\sum_{\mathbf{k},s}\omega_k|\boldsymbol{\mu}_{21}\cdot\mathbf{f}_{\mathbf{k}s}(\mathbf{h})|^2\int_0^{t-t_0}d\tau\, e^{i(\omega_k-\omega_a)\tau}+\text{c.c.} \tag{2.6}$$

In deriving (2.5) we have made use of the following identities for the spin matrices:

$$[\sigma^{+},\sigma_z]_+=[\sigma^{-},\sigma_z]_+=0\ ,$$

$$[\sigma^{+},\sigma^{-}-\sigma^{+}]_+=-[\sigma^{-},\sigma^{-}-\sigma^{+}]_+=1\ .$$

With suitable approximation and renormalization, the term $\beta(\mathbf{h})$ gives the atomic linewidth and energy shift[10] (in the absence of squeezing). We will not be concerned with the evaluation of $\beta(\mathbf{h})$, however.

Next, we move to a frame rotating at frequency Ω. Defining input quadrature phases by

$$\mathbf{E}^{\perp}_{\text{in}}(\mathbf{h},t)=\mathbf{X}_{\text{in}}(\mathbf{h},t)\sin(\Omega t-\alpha)+\mathbf{Y}_{\text{in}}(\mathbf{h},t)\cos(\Omega t-\alpha)\ , \tag{2.7}$$

we make the usual rotating-wave approximation, and after some manipulation of the equations we arrive finally at (choosing $\alpha=\pi$)

$$\begin{aligned}
\dot{\sigma}_x&=-(\omega_a-\Omega)\sigma_y-\frac{1}{2\hbar}\boldsymbol{\mu}_{21}\cdot[\mathbf{X}_{\text{in}}(\mathbf{h},t),\sigma_z]_+\ ,\\
\dot{\sigma}_y&=(\omega_a-\Omega)\sigma_x-\frac{1}{2\hbar}\boldsymbol{\mu}_{21}\cdot[\mathbf{Y}_{\text{in}}(\mathbf{h},t),\sigma_z]_+\ ,\\
\dot{\sigma}_z&=-\beta(\mathbf{h})+\frac{1}{2\hbar}\boldsymbol{\mu}_{21}\cdot[\mathbf{X}_{\text{in}}(\mathbf{h},t),\sigma_x]_+ +\frac{1}{2\hbar}\boldsymbol{\mu}_{21}\cdot[\mathbf{Y}_{\text{in}}(\mathbf{h},t),\sigma_y]_+\ ,
\end{aligned} \tag{2.8}$$

where $\sigma_x=\sigma^{-}+\sigma^{+}$ and $\sigma_y=i(\sigma^{-}-\sigma^{+})$. These equations are of the form derived and used by Parkins and Gardiner[7] in their analysis of the effect of finite-bandwidth squeezing. Following their treatment we can define operators

$$\beta_X(t)\rho\equiv\tfrac{1}{2}\boldsymbol{\mu}_{21}\cdot[\mathbf{X}_{\text{in}}(\mathbf{h},t),\rho]_+\ ,$$

$$\beta_Y(t)\rho\equiv\tfrac{1}{2}\boldsymbol{\mu}_{21}\cdot[\mathbf{Y}_{\text{in}}(\mathbf{h},t),\rho]_+\ ,$$

which, owing to their properties of commutativity, can be treated as classical noise sources. The statistics of $\beta_X(t)$ and $\beta_Y(t)$, as defined by the correlation functions $\langle\beta_X(t)\beta_X(t')\rangle$ and $\langle\beta_Y(t)\beta_Y(t')\rangle$, will then determine the behavior of $\langle\sigma_{x,y,z}(t)\rangle$ and, in particular, whether or not the decay of one of $\langle\sigma_x(t)\rangle$ and $\langle\sigma_y(t)\rangle$ can be inhibited. The dependence of the atomic dipole decay on the surrounding mode structure is now explicitly included in $\boldsymbol{\mu}_{21}\cdot\mathbf{Y}_{\text{in}}(\mathbf{h},t)$ [and $\boldsymbol{\mu}_{21}\cdot\mathbf{X}_{\text{in}}(\mathbf{h},t)$], which we write for completeness

$$\boldsymbol{\mu}_{21}\cdot\mathbf{Y}_{\text{in}}(\mathbf{h},t)=i\sum_{\mathbf{k},s}\left[\frac{\hbar\omega_k}{2}\right]^{1/2}a_{\mathbf{k}s}(t_0)e^{-i(\omega_k-\Omega)t} \times[\boldsymbol{\mu}_{21}\cdot\mathbf{f}_{\mathbf{k}s}(\mathbf{h})]+\text{H.c.} \tag{2.9}$$

Specification of the correlation functions will of course require specifications of, for instance, $\langle a_{\mathbf{k}s}(t_0)a_{\mathbf{k}'s'}(t_0)\rangle$ for a squeezed input field, incident over some finite solid angle. We shall consider this later.

III. MODE FUNCTIONS OF THE CAVITY

Firstly, however, we shall consider the mode functions appropriate to the plane-mirror Fabry-Pérot configuration (Fig. 1) we are contemplating. These give the spatial dependence of the field, and can be computed using classical electromagnetic theory. The two plane mirrors lie parallel to the xy plane, the first a perfectly reflecting mirror at $z=0$, and the second a partially transmitting lossless mirror at $z=L$, with real reflectivity R, and transmittivity $i(1-R^2)^{1/2}$ (same for both directions). We assume that the mirrors are very large, so that end effects can be ignored.

By a consideration of boundary conditions at the mirrors,[11,12] we derive the following expression for the mode functions inside the cavity

$$\mathbf{f}_{\mathbf{k}s}(\mathbf{r})=V^{-1/2}g(k_z)(\boldsymbol{\epsilon}_{\mathbf{k}s}e^{i\mathbf{k}\cdot\mathbf{r}}+\boldsymbol{\epsilon}'_{\mathbf{k}s}e^{-i\mathbf{k}'\cdot\mathbf{r}})\ , \tag{3.1}$$

where V is the quantization volume, and $g(k_z)$ is taken to have the form

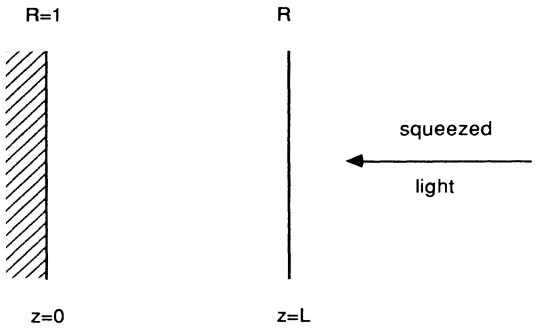

FIG. 1. Cavity configuration.

$$g(k_z)=\frac{i(1-R^2)^{1/2}}{1-Re^{-i2k_zL}} . \tag{3.2}$$

Outside the cavity, the mode functions have the form

$$\mathbf{f}_{\mathbf{k}s}(\mathbf{r})=V^{-1/2}[\boldsymbol{\epsilon}_{\mathbf{k}s}e^{i\mathbf{k}\cdot\mathbf{r}}+h(k_z)\boldsymbol{\epsilon}'_{\mathbf{k}s}e^{i\mathbf{k}'\cdot\mathbf{r}}] , \tag{3.3}$$

where

$$h(k_z)=-\left[\frac{1-Re^{i2k_zL}}{1-Re^{-i2k_zL}}\right] . \tag{3.4}$$

We have assumed that the reflectivity R is the same for both polarizations. The polarization vector $\boldsymbol{\epsilon}_{\mathbf{k}s}$, and the wave vector $\mathbf{k}$, can be written as a sum of components parallel and perpendicular to the xy plane, respectively,

$$\boldsymbol{\epsilon}_{\mathbf{k}s}=\boldsymbol{\epsilon}^{\perp}_{\mathbf{k}s}+\boldsymbol{\epsilon}^{\parallel}_{\mathbf{k}s},\quad \mathbf{k}=\mathbf{k}^{\perp}+\mathbf{k}^{\parallel} . \tag{3.5}$$

The primed quantities in (3.1) and (3.3) are then defined as

$$\boldsymbol{\epsilon}'_{\mathbf{k}s}=\boldsymbol{\epsilon}^{\perp}_{\mathbf{k}s}-\boldsymbol{\epsilon}^{\parallel}_{\mathbf{k}s},\quad \mathbf{k}'=-\mathbf{k}^{\perp}+\mathbf{k}^{\parallel} . \tag{3.6}$$

We note that the following identities hold: $\mathbf{k}\cdot\boldsymbol{\epsilon}=\mathbf{k}'\cdot\boldsymbol{\epsilon}'=0$, $\boldsymbol{\epsilon}\cdot\boldsymbol{\epsilon}^*=\boldsymbol{\epsilon}'\cdot\boldsymbol{\epsilon}'^*=1$.

For our purposes, we need only know the mode functions inside and outside of the cavity. For a precise check on the orthogonality of the mode functions, one must of course, take account of the partially transmitting mirror. In the case of an infinitely thin mirror, this necessitates an additional surface term in the orthogonality integral.[12] If the mirror is given a finite thickness and finite dielectric constant, an approach such as is used in Ref. 13 for the quantization of fields about an interface is then required.

The effect of the cavity is most clearly exhibited in the form of $|g(k_z)|^2$, which we identify as the Airy function of the cavity

$$|g(k_z)|^2=\frac{1-R^2}{(1-R)^2+4R\sin^2(k_zL)} . \tag{3.7}$$

If R is close to 1, then this function displays a series of sharp peaks for angles of incidence such that $\sin(k_zL)=\sin(kL\cos\theta_k)=0$. If, therefore, $L=\lambda/2$, the function given in (3.7) will exhibit a peak centered at $\cos\theta_k=1$ (the peak at $\cos\theta_k=0$ can be ignored, as other factors that enter our calculations later are zero at this angle), that is, a strong coupling is effected only with those modes in a small solid angle about the z axis, (i.e., perpendicular to the mirrors). In the next section we shall examine the requirements for producing an effective squeezing of these modes.

IV. SQUEEZED-VACUUM INPUT

The formulation of squeezing in a full three-dimensional electromagnetic field has not been considered before, so it seems appropriate to set this out with some care. In a one-dimensional situation, a multimode squeezed state can be specified by operators $A(\omega)$, $A^{\dagger}(\omega)$, such that

$$\begin{aligned}&[A(\omega),A^{\dagger}(\omega')]=\delta(\omega-\omega') ,\\ &\langle A^{\dagger}(\omega)A(\omega')\rangle=\delta(\omega-\omega')N(\omega) ,\\ &\langle A(\omega)A(\omega')\rangle=\delta(2\Omega-\omega-\omega')M(\omega) ,\end{aligned} \tag{4.1}$$

where Ω is the central frequency about which squeezing takes place. To generalize this to three dimensions, let us define an operator analogous to $A(\omega)$,

$$A(k)=\sum_{\hat{\mathbf{k}},s}\alpha^*_s(\mathbf{k})a_{\mathbf{k}s} , \tag{4.2}$$

with

$$\sum_{\hat{\mathbf{k}},s}|\alpha_s(\mathbf{k})|^2=1 , \tag{4.3}$$

where $\hat{\mathbf{k}}$ is a unit vector in the direction of $\mathbf{k}$. We want the same kind of relations as for $A(\omega)$ to be true. But further, let us specify that the field is not squeezed in any other modes. This can be achieved by defining the state by

$$[a_{\mathbf{k}s},a^{\dagger}_{\mathbf{k}',s'}]=\delta^3_{\mathbf{k},\mathbf{k}'}\delta_{s,s'} , \tag{4.4}$$

$$\begin{aligned}&\langle a^{\dagger}_{\mathbf{k}s}a_{\mathbf{k}',s'}\rangle=N(k-K)\alpha^*_s(\mathbf{k})\alpha_{s'}(\mathbf{k}')\delta_{k,k'}\delta_{s,s'} ,\\ &\langle a_{\mathbf{k}s}a_{\mathbf{k}'s'}\rangle=M(k-K)\alpha_s(\mathbf{k})\alpha_{s'}(\mathbf{k}')\delta_{k,2K-k'}\delta_{s,s'} ,\end{aligned} \tag{4.5}$$

where $K=\Omega/c$. In this case, we can see

$$\begin{aligned}&\langle A^{\dagger}(k)A(k')\rangle=N(k-K)\delta_{k,k'} ,\\ &\langle A(k)A(k')\rangle=M(k-K)\delta_{k,2K-k'} .\end{aligned} \tag{4.6}$$

However, if

$$B(k)=\sum_{\hat{\mathbf{k}},s}\beta^*_s(\mathbf{k})a_{\mathbf{k}s} , \tag{4.7}$$

and

$$\sum_{\hat{\mathbf{k}},s}\alpha_s(\mathbf{k})\beta^*_s(\mathbf{k})=0 , \tag{4.8}$$

then the operator $B(k)$ is not squeezed, and indeed has no excitation in it at all. Thus the definitions (4.4) and (4.5) represent a situation in which there is squeezing only between modes with wave function $\alpha_s(\mathbf{k})$.

A. Ideal matching

Gardiner[1] considered the case of an atom in free space, noting that $\alpha_s(\mathbf{k})$ should, in that case, correspond as

closely as possible to an electric dipole wave, with Ω_{sq}, the solid angle over which the input is squeezed, approximately 4π, giving the maximum overlap of $\alpha_s(\mathbf{k})$ with $\boldsymbol{\mu}_{21}\cdot\mathbf{f}_{\mathbf{k}s}(\mathbf{h})$. Similarly, we may attempt to maximize this overlap for our particular situation by choosing

$$\alpha_s(\mathbf{k})=\mathcal{N}^{-1/2}\boldsymbol{\mu}_{21}^*\cdot\mathbf{f}_{\mathbf{k}s}^*(\mathbf{h}_0)\ , \tag{4.9}$$

where

$$\mathcal{N}=\int_{\Omega_{sq}} d\Omega_k \sum_s |\boldsymbol{\mu}_{21}\cdot\mathbf{f}_{\mathbf{k}s}(\mathbf{h}_0)|^2\ ,$$

and $\mathbf{h}_0=(0,0,h_z)$. A choice such as (4.9) is important, otherwise the phase of the squeezing can be altered to an extent that a significant reduction in fluctuations is no longer possible. In simple terms, the mode structure of the squeezing incident upon the cavity should match as closely as possible to the mode structure of the cavity in which we aim to carry out the experiment. In practice, some approximation will be necessary, but for the moment we consider the "ideal" case (4.9). Later we shall examine other possible choices of $\alpha_s(\mathbf{k})$, at which stage the importance of matching will be emphasized more definitively.

Computation of the correlation function $\langle\beta_Y(t)\beta_Y(t')\rangle$, from which we may solve for the decay rate of $\langle\sigma_y\rangle$, proceeds as follows. If ρ_b is the bath density operator, then, using the properties of the trace, one can write

$$\begin{aligned}\langle\beta_Y(t)\beta_Y(t')\rangle &\equiv \mathrm{Tr}_b[\beta_Y(t)\beta_Y(t')\rho_b]\\ &=\tfrac{1}{4}\mathrm{Tr}_b\{[\boldsymbol{\mu}_{21}\cdot\mathbf{Y}_{\mathrm{in}}(\mathbf{h},t),[\boldsymbol{\mu}_{21}\cdot\mathbf{Y}_{\mathrm{in}}(\mathbf{h},t'),\rho_b]_+]_+\}\\ &=\tfrac{1}{2}\mathrm{Tr}_b\{[\boldsymbol{\mu}_{21}\cdot\mathbf{Y}_{\mathrm{in}}(\mathbf{h},t),\boldsymbol{\mu}_{21}\cdot\mathbf{Y}_{\mathrm{in}}(\mathbf{h},t')]_+\rho_b\}\\ &\equiv\tfrac{1}{2}\langle[\boldsymbol{\mu}_{21}\cdot\mathbf{Y}_{\mathrm{in}}(\mathbf{h},t),\boldsymbol{\mu}_{21}\cdot\mathbf{Y}_{\mathrm{in}}(\mathbf{h},t')]_+\rangle\ .\end{aligned} \tag{4.10}$$

Using (2.9) and (4.5), and moving to an integral representation (for the necessary modifications to our discrete expressions see, for example, Ref. 14), we derive

$$\begin{aligned}\langle\beta_Y(t)\beta_Y(t')\rangle=&-\frac{V}{(2\pi)^3}\frac{\hbar c}{2}\sum_s\int_0^{2K}dk\,k^2[k(2K-k)]^{1/2}e^{-ic(k-K)(t-t')}M(k-K)\\ &\times\int_{\Omega_{sq}}d\Omega_k\int_{\Omega_{sq}}d\Omega_{k'}\alpha_s(\mathbf{k})[\boldsymbol{\mu}_{21}\cdot\mathbf{f}_{\mathbf{k}s}(\mathbf{h})]\alpha_s(\mathbf{k}')[\boldsymbol{\mu}_{21}\cdot\mathbf{f}_{\mathbf{k}'s}(\mathbf{h})]\\ &+\mathrm{c.c.}+\frac{V}{(2\pi)^3}\frac{\hbar c}{2}\sum_s\int_0^{\infty}dk\,k^3e^{ic(k-K)(t-t')}N(k-K)\\ &\times\int_{\Omega_{sq}}d\Omega_k\int_{\Omega_{sq}}d\Omega_{k'}\alpha_s^*(\mathbf{k})[\boldsymbol{\mu}_{21}^*\cdot\mathbf{f}_{\mathbf{k}s}^*(\mathbf{h})]\alpha_s(\mathbf{k}')[\boldsymbol{\mu}_{21}\cdot\mathbf{f}_{\mathbf{k}'s}(\mathbf{h})]+\mathrm{c.c.}\\ &+\frac{V}{(2\pi)^3}\frac{\hbar c}{2}\int_0^{\infty}dk\,k^3e^{-ic(k-K)(t-t')}\int_{\text{half-sphere}}d\Omega_k\sum_s|\boldsymbol{\mu}_{21}\cdot\mathbf{f}_{\mathbf{k}s}(\mathbf{h})|^2\ ,\end{aligned} \tag{4.11}$$

where $\mathbf{k}'\equiv k\hat{\mathbf{k}}'$. We move via Fourier transform to k space (frequency space), substitute (4.9) for $\alpha_s(\mathbf{k})$, and evaluate what results at $k=K=\Omega/c$, the central squeezing wave number,

$$\begin{aligned}\langle\beta_Y(k)\beta_Y(k')\rangle=&-\frac{V}{(2\pi)^3}\frac{\hbar K^3}{2}M(K)\sum_s\frac{1}{\mathcal{N}}\left[\int_{\Omega_{sq}}d\Omega_k[\boldsymbol{\mu}_{21}^*\cdot\mathbf{f}_{\mathbf{K}s}^*(\mathbf{h}_0)][\boldsymbol{\mu}_{21}\cdot\mathbf{f}_{\mathbf{K}s}(\mathbf{h})]\right]^2\delta(k+k')+\mathrm{c.c.}\\ &+\frac{V}{(2\pi)^3}\frac{\hbar K^3}{2}N(K)\sum_s\frac{1}{\mathcal{N}}\left|\int_{\Omega_{sq}}d\Omega_k[\boldsymbol{\mu}_{21}^*\cdot\mathbf{f}_{\mathbf{K}s}^*(\mathbf{h}_0)][\boldsymbol{\mu}_{21}\cdot\mathbf{f}_{\mathbf{K}s}(\mathbf{h})]\right|^2\delta(k+k')+\mathrm{c.c.}\\ &+\frac{V}{(2\pi)^3}\frac{\hbar K^3}{2}\int_{\text{half-sphere}}d\Omega_k\sum_s|\boldsymbol{\mu}_{21}\cdot\mathbf{f}_{\mathbf{K}s}(\mathbf{h})|^2\delta(k+k')\ ,\end{aligned} \tag{4.12}$$

where by $\mathbf{K}$ we mean $\mathbf{K}=K\hat{\mathbf{k}}$. To carry out the polarization sum, it is convenient to use the circular polarization vectors

$$\begin{aligned}\boldsymbol{\epsilon}_{\mathbf{k}+}&=-\frac{1}{\sqrt{2}}(-\cos\theta_k\cos\phi_k+i\sin\phi_k,-\cos\theta_k\sin\phi_k-i\cos\phi_k,\sin\theta_k)e^{i\phi_k}\ ,\\ \boldsymbol{\epsilon}_{\mathbf{k}-}&=\frac{1}{\sqrt{2}}(-\cos\theta_k\cos\phi_k-i\sin\phi_k,-\cos\theta_k\sin\phi_k+i\cos\phi_k,\sin\theta_k)e^{-i\phi_k}\ .\end{aligned} \tag{4.13}$$

With this particular choice, the polarizations are unique when $\theta_k=0$ (i.e., the same for any ϕ_k).

We shall assume that with suitable optical pumping the atoms can be prepared in a state from which only a $\Delta M=\pm1$ transition is possible (Jhe *et al.*[8]). For our cavity configuration, this shall correspond to transitions in which the emitted photons are polarized in a plane parallel to the mirror surfaces (i.e., the atom quantization axis is chosen as the normal to the mirrors), and for which the dipole moment can be written[15]

$$\boldsymbol{\mu}_{21}=\frac{\mu_{21}}{\sqrt{2}}(1,i,0) . \tag{4.14}$$

We then find

$$\boldsymbol{\mu}_{21}\cdot\mathbf{f}_{\mathbf{K}+}(\mathbf{h})=-i\sqrt{1/V}\,\mu_{21}g(K_z)(1-\cos\theta_k)e^{i2\phi_k}\sin(Kh_z\cos\theta_k)\exp[iK(h_x\sin\theta_k\cos\phi_k+h_y\sin\theta_k\sin\phi_k)] , \tag{4.15}$$

$$\boldsymbol{\mu}_{21}\cdot\mathbf{f}_{\mathbf{K}-}(\mathbf{h})=-i\sqrt{1/V}\,\mu_{21}g(K_z)(1+\cos\theta_k)\sin(Kh_z\cos\theta_k)\exp[iK(h_x\sin\theta_k\cos\phi_k+h_y\sin\theta_k\sin\phi_k)] . \tag{4.16}$$

We note at this point that with $|g(K_z)|^2$ sharply peaked about $\cos\theta_k=1$, the dominant contribution to the quantities we compute will come from terms involving $\boldsymbol{\mu}_{21}\cdot\mathbf{f}_{\mathbf{K}-}(\mathbf{h})$ [rather than $\boldsymbol{\mu}_{21}\cdot\mathbf{f}_{\mathbf{K}+}(\mathbf{h})$, which is small], that is, from only a single polarization.

To simplify matters we set $h_y=0$, so that we shall be considering variations in the atom's position along the x axis [from the "central squeezing position" $\mathbf{h}_0=(0,0,h_z)$]. By varying h_x, we will be able to gauge the area inside the cavity over which reduced fluctuations can be achieved.

The solid angle over which the squeezing shall be incident is defined by

$$\int_{\Omega_{sq}}d\Omega_k\equiv\int_0^{\theta_2}d\theta_k\sin\theta_k\int_0^{2\pi}d\phi_k , \tag{4.17}$$

that is, we consider a cone centered on the z axis. After some calculation, and a change of integration variable ($u=\cos\theta_k$), we produce [with $N\equiv N(K)$, $M\equiv M(K)$]

$$\begin{aligned}
&\langle\beta_Y(k)\beta_Y(k')\rangle/\delta(k+k') \\
&=\frac{\hbar\mu_{21}^2K^3}{8\pi^2}(N-M)\frac{1+R}{1-R}\frac{1}{\mathcal{N}'}\left[\int_{\cos\theta_2}^1du\,(1-u)^2\frac{\sin^2(Kh_zu)}{1+F\sin^2(KLu)}J_0(Kh_x(1-u^2)^{1/2})\right]^2 \\
&+\frac{\hbar\mu_{21}^2K^3}{8\pi^2}(N-M)\frac{1+R}{1-R}\frac{1}{\mathcal{N}'}\left[\int_{\cos\theta_2}^1du\,(1+u)^2\frac{\sin^2(Kh_zu)}{1+F\sin^2(KLu)}J_0(Kh_x(1-u^2)^{1/2})\right]^2 \\
&+\frac{\hbar\mu_{21}^2K^3}{4\pi^2}\frac{1+R}{1-R}\int_0^1du(1+u^2)\frac{\sin^2(Kh_zu)}{1+F\sin^2(KLu)} \\
&=\frac{\hbar\mu_{21}^2K^3}{6\pi^2}B(\mathbf{h}) ,
\end{aligned} \tag{4.18}$$

where $F=4R/(1-R)^2$, J_0 is the zeroth-order Bessel function, and now

$$\mathcal{N}'=\int_{\cos\theta_2}^1du\,(1+u^2)\frac{\sin^2(Kh_zu)}{1+F\sin^2(KLu)} . \tag{4.19}$$

For reference back to the original equations of motion, it follows from (4.18) that

$$\langle\beta_Y(t)\beta_Y(t')\rangle=\frac{\hbar\mu_{21}^2K^3}{6\pi^2}B(\mathbf{h})\delta(t-t') , \tag{4.20}$$

and hence that

$$\langle\dot{\sigma}_y\rangle=(\omega_a-\Omega)\langle\sigma_x\rangle-\gamma B(\mathbf{h})\langle\sigma_y\rangle , \tag{4.21}$$

where γ is the free-space spontaneous-emission rate. Under free-space conditions, $B(\mathbf{h})$ is equal to $\frac{1}{2}$.

The integrals appearing in (4.18) and (4.19) can be evaluated by numerical integration. To obtain some estimate by analytical means, we can set $h_x=0$, and approximate the sharply peaked Airy function by a Lorentzian. We further assume that the other factors in the integrands do not vary significantly over the width of this Lorentzian, and hence that they can be removed from the integral and set equal to their values at $u=1$. Considering the case where $KL=\pi$ ($L=\lambda/2$), and $Kh_z=\pi/2$ (i.e., the atom is at the center of the cavity), we find

$$\begin{aligned}
&B(h_x=0,\,h_z=L/2) \\
&\simeq\frac{3}{\pi}\frac{1+R}{\sqrt{R}}\{\tfrac{1}{2}\tan^{-1}(\pi\sqrt{F}) \\
&\qquad+(N-M)\tan^{-1}[\pi\sqrt{F}(1-\cos\theta_2)]\} ,
\end{aligned} \tag{4.22}$$

where, for an ideal parametric oscillator producing broadband squeezed light, $M=[N(N+1)]^{1/2}$ (Refs. 16 and 17), so that for good squeezing $N-M$ approaches $-\frac{1}{2}$. Hence, choosing $\cos\theta_2=0$ the term in curly brackets may become very small. However, if F is large, this requirement may be relaxed; for instance, if $R=0.98$, and $\theta_2=0.3$ rad, then $\tan^{-1}(\pi\sqrt{F})=1.57$, while

$$\tan^{-1}[\pi\sqrt{F}(1-\cos\theta_2)]=1.50 ,$$

that is, a substantial reduction in fluctuations is still possible at the point we have chosen midway between the mirrors.

Numerical results

The results of computer evaluation of $B(\mathbf{h})$, as defined in Eqs. (4.18) and (4.19), are shown in Figs. 2 and 3. In Fig. 2 we display four plots for $L=\lambda/2$, $R=0.99$, and $N-M=-\frac{15}{32}$ (94% squeezing), with $\theta_2=0$, 0.1, 0.3, and

1.0 rad, respectively. As one can see there is relatively little variation in going from $\theta_2=0.1$ to $\theta_2=1.0$, emphasizing the function of the cavity in isolating those modes nearly perpendicular to the mirrors. The maximum reduction in fluctuations relative to the vacuum occurs in each case at $h_z/L=0.5$, $h_x/L=0$. These reductions are 76%, 92%, and 93.7% for $\theta_2=0.1$, 0.3, and 1.0, respectively. Hence, for $\theta_2 \gtrsim 0.3$, with $R=0.99$, the reductions possible are limited essentially by the available squeezing.

A good amount of squeezing is available in the x direction for several times the width L of the cavity. This "width" of squeezing depends on the reflectivity R, as shown in Fig. 3, where we consider $\theta_2=0.3$ with $R=0.95$ and $R=0.995$. With increasing R, the area over which significant squeezing occurs increases considerably. We note, in addition, that significant reductions are possible with fairly modest values of the reflectivity R, as demonstrated in Fig. 3(a). In terms of the maximum achievable inhibition, a decrease in R may be compensated for by an increase in the angular limit θ_2 of the squeezed input. For instance, with $R=0.95$, and with the same input squeezing as above, a maximum reduction of 93% is possible with $\theta_2=1.0$, as opposed to 84% with $\theta_2=0.3$.

As an aside, we note that in the limit $R \to 1$, with $N=M=0$, the quantity $B(h_z=L/2)$ approaches 1.5. This is equivalent to a spontaneous-emission rate three times greater than the free-space rate, in agreement with previous analyses of,[18] and experiments testing,[19] the decay rates of atoms between plane parallel perfect mirrors separated by half a wavelength.

It is important to consider also the sensitivity of the effects to small changes in the mirror spacing L. This will be very pertinent to any practical experimental arrangement as the distances involved are extremely small. For $L<\lambda/2$, the mode density inside the cavity is greatly diminished, and we enter the regime of inhibited spon-

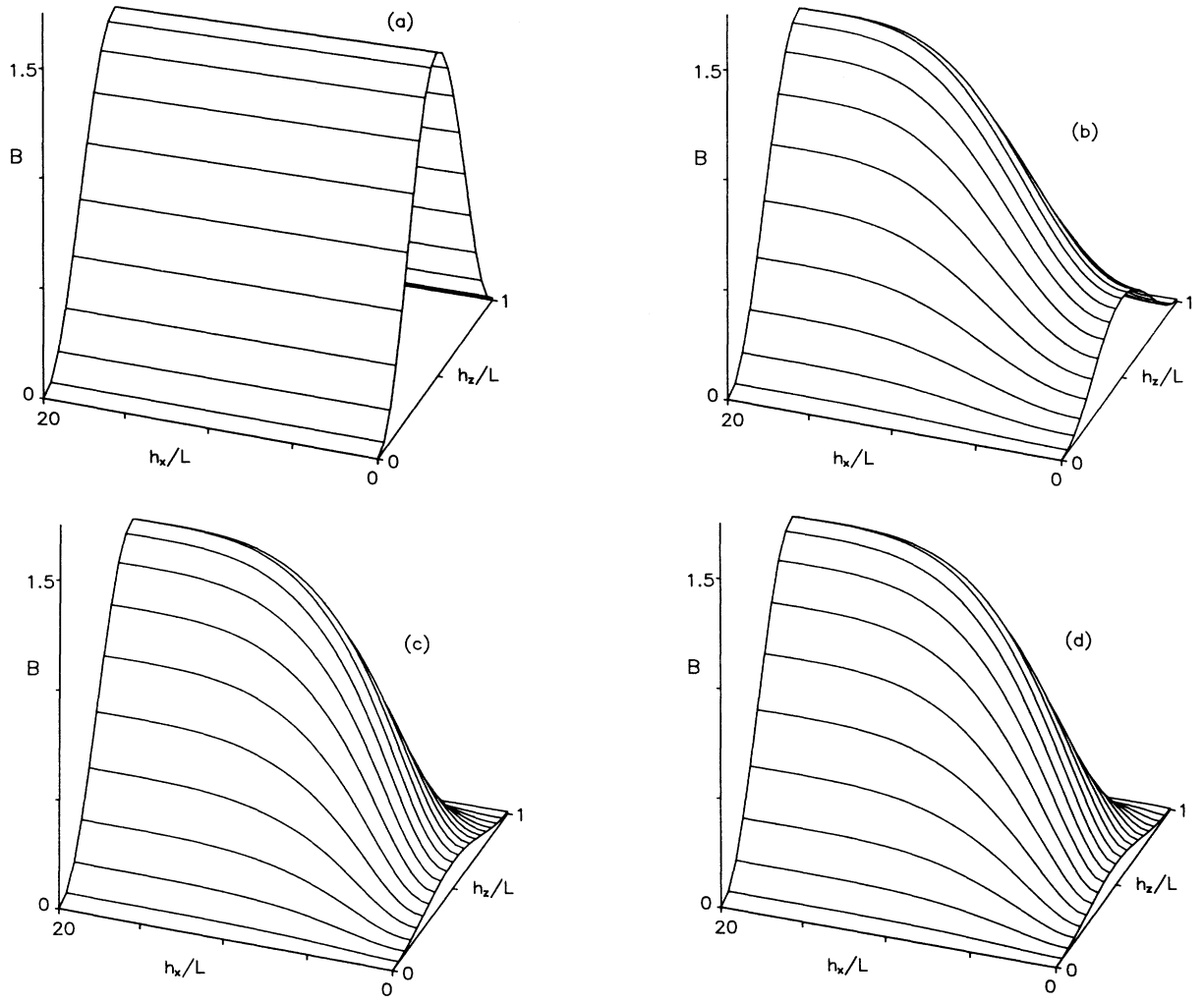

FIG. 2. B as a function of x and z coordinates, for $L=\lambda/2$, $R=0.99$, and $N-M=-\frac{15}{32}$, with (a) $\theta_2=0$, (b) $\theta_2=0.1$, (c) $\theta_2=0.3$, (d) $\theta_2=1.0$.

taneous emission (remember that the dipole moment is parallel to the mirrors).

In Fig. 4 we display the result, with squeezing, for $L=0.495\lambda$. In all regions, the decay rate is significantly reduced from the free-space rate. The effect of squeezing can still be seen for sufficiently small h_x/L, however, the maximum relative reduction in B (78%) is less than that obtained with the same parameters for $L=\lambda/2$ (92%). Clearly, also, the absolute difference between the results obtained with and without squeezing is much smaller than for $L=\lambda/2$.

For smaller values of R, the cutoff in mode density is less sharp, and the drop-off in decay rate due to inhibited spontaneous emission is somewhat less dramatic. However, the effects of reducing L below $\lambda/2$ are clearly undesirable if one hopes to see a large absolute reduction in the decay rate as a consequence of squeezing.

If L is slightly greater than $\lambda/2$, we find that significant further enhancement of the decay rate, both with and without squeezing, is possible. This occurs as the remainder of the first-order Fabry-Pérot maximum

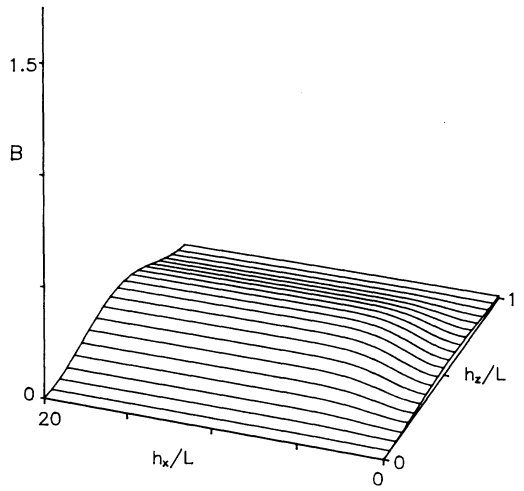

FIG. 4. B as a function of x and z coordinates, for $L=0.495\lambda$, $R=0.99$, $N-M=-\frac{15}{32}$, and $\theta_2=0.3$.

(i.e., the peak of the Airy function) is incorporated in the integral of (4.18). Where squeezing is not significant, $B(h_z=L/2)$ now approaches 3, as shown in Fig. 5, where we consider the case $R=0.99$, $L/\lambda=0.51$. As L is increased beyond this value, this enhancement is reduced, with the next maximum occurring around $L/\lambda=1$. The maximum reduction due to squeezing ($N-M=-\frac{15}{32}$, $\theta_2=0.3$) is 92%, the same as was found with $L=\lambda/2$. The inhibition does not persist over as large an area as before, but the advantage now is that the absolute magnitude of the reduction is increased.

For lower values of R, a graph similar to that in Fig. 5 is found, but with the maximum inhibition at $h_x=0$ reduced (with increased θ_2, this may be improved).

If L is too much greater than $\lambda/2$ (greater than ~ 0.52 for $R=0.99$), an increase in θ_2 (from 0.3 rad) is needed to maintain a significant inhibition. We demonstrate this in Fig. 6, where we display the results for $L/\lambda=0.525$, and

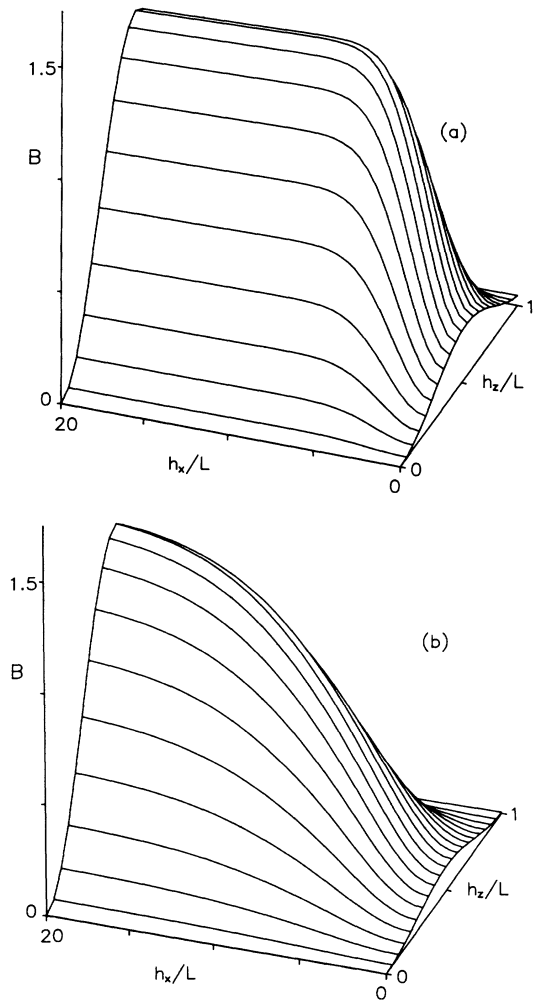

FIG. 3. B as a function of x and z coordinates, for $L=\lambda/2$, $\theta_2=0.3$, $N-M=-\frac{15}{32}$, with (a) $R=0.95$, (b) $R=0.995$.

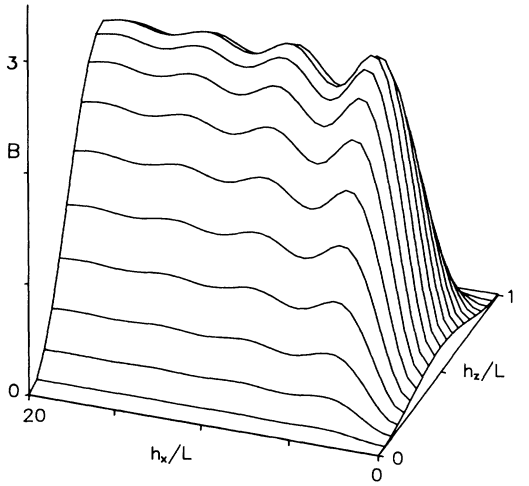

FIG. 5. B as a function of x and z coordinates, for $L=0.51\lambda$, $R=0.99$, $N-M=-\frac{15}{32}$, and $\theta_2=0.3$.

$R=0.99$, with $\theta_2=0.3$ and $\theta_2=1.0$. These results emphasize the importance of matching the input to the cavity over a sufficiently large solid angle.

In conclusion, there appears to be a reasonable range over which L may be varied and yet allow a significant reduction in the decay rate B relative to the normal vacuum level. This range is biased towards values of L equal to or slightly larger than $\lambda/2$, as opposed to values of L less than $\lambda/2$, where inhibited spontaneous emission becomes the dominant effect.

B. Nonideal matching

In practice, a perfectly matched input may not be possible, so it is important to repeat our calculations with $\alpha_s(\mathbf{k})$ given not by (4.9), but rather by some approximation to that function. It is instructive to consider the form of the exact mode function; if R is close to 1 then, to a good approximation

$$\begin{aligned}\boldsymbol{\mu}_{21}\cdot\mathbf{f}_{\mathbf{K}+}(\mathbf{h}_0)&\simeq 0\ ,\\ \boldsymbol{\mu}_{21}\cdot\mathbf{f}_{\mathbf{K}-}(\mathbf{h}_0)&\simeq -2i\left[\frac{1}{V}\right]^{1/2}\mu_{21}\sin(K_z h_z)g(K_z)\ ,\end{aligned}\tag{4.23}$$

from which it is clear that we must try to match the function $g(K_z)$, as given by (3.2), for a particular polarization. We choose a Gaussian distribution over angle as an example of an approximate match, which will enable us to check how critical the requirement of matching is. In

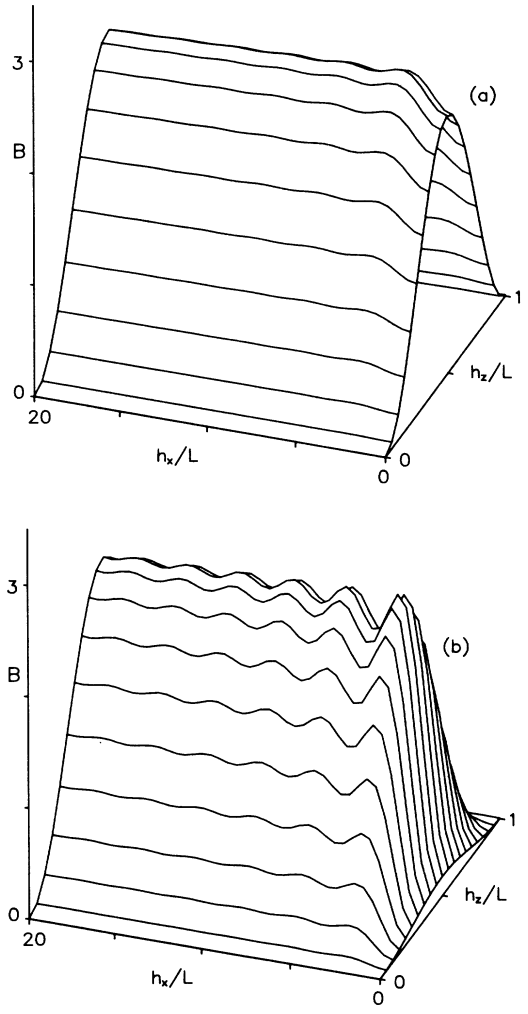

FIG. 6. B as a function of x and z coordinates, for $L=0.525\lambda$, $R=0.99$, $N-M=-\frac{15}{32}$, with (a) $\theta_2=0.3$, (b) $\theta_2=1.0$.

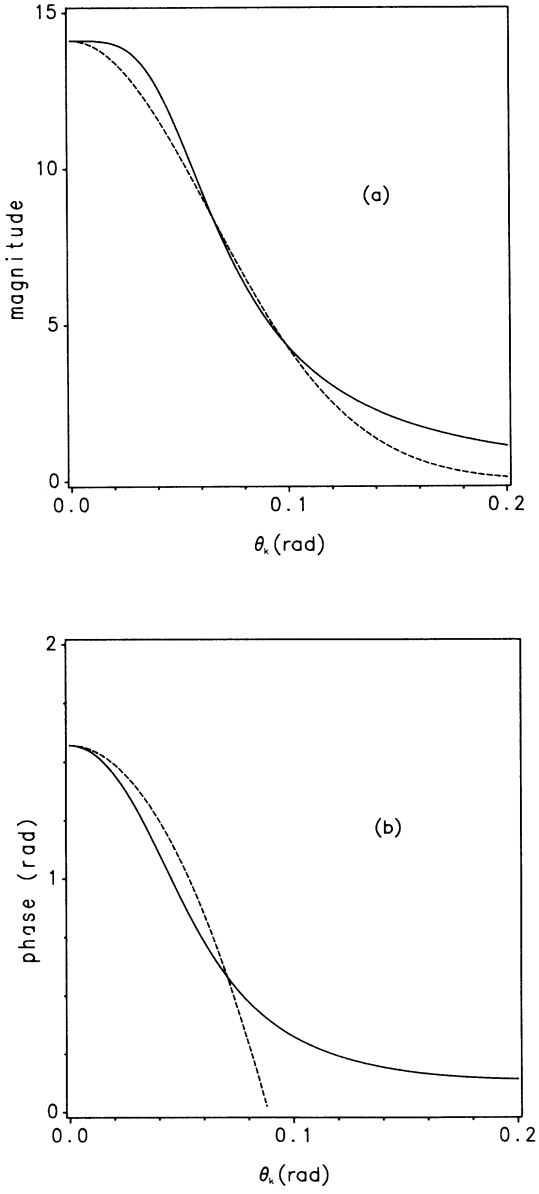

FIG. 7. (a) Magnitude and (b) phase of $g(K_z)$ (solid lines) for $L=\lambda/2$, $R=0.99$, compared with $14\exp(-120\sin^2\theta_k)$ and $\pi/2-200\sin^2\theta_k$ (dashed lines), respectively.

particular, we choose

$$\alpha_-(\mathbf{k})=0\ ,$$
$$\alpha_+(\mathbf{k})=\mathcal{N}_g^{-1/2}\exp[-\delta\sin^2\theta_k - i(\eta+\xi\sin^2\theta_k)] \times i\sin(K_z h_z)\ , \tag{4.24}$$

where δ, η, and ξ are real constants, and the normalization factor

$$\mathcal{N}_g=\int_{\Omega_{sq}} d\Omega_k \exp(-2\delta\sin^2\theta_k)\sin^2(Kh_z\cos\theta_k)\ , \tag{4.25}$$

with $\int_{\Omega_{sq}} d\Omega_k$ as defined in (4.17). This form may be considered to model a focused Gaussian beam in the paraxial approximation.[20]

A comparison of the magnitude and phase of $g(K_z)$ with $\exp(-\delta\sin^2\theta_k)$ (appropriately scaled) and $(\eta+\xi\sin^2\theta_k)$, respectively, is shown in Fig. 7, for $R=0.99$, and $L=\lambda/2$, with $\delta=120$, $\eta=\pi/2$, and $\xi=-200$ (a particular choice of parameters we shall consider later). The Lorentzian-type long-time tails of $g(K_z)$ are not well matched, but in the more important small-angle region, where $g(K_z)$ is sharply peaked, the approximation is much better.

Using the expressions (4.24) for $\alpha_\pm(\mathbf{k})$ in (4.11), we obtain

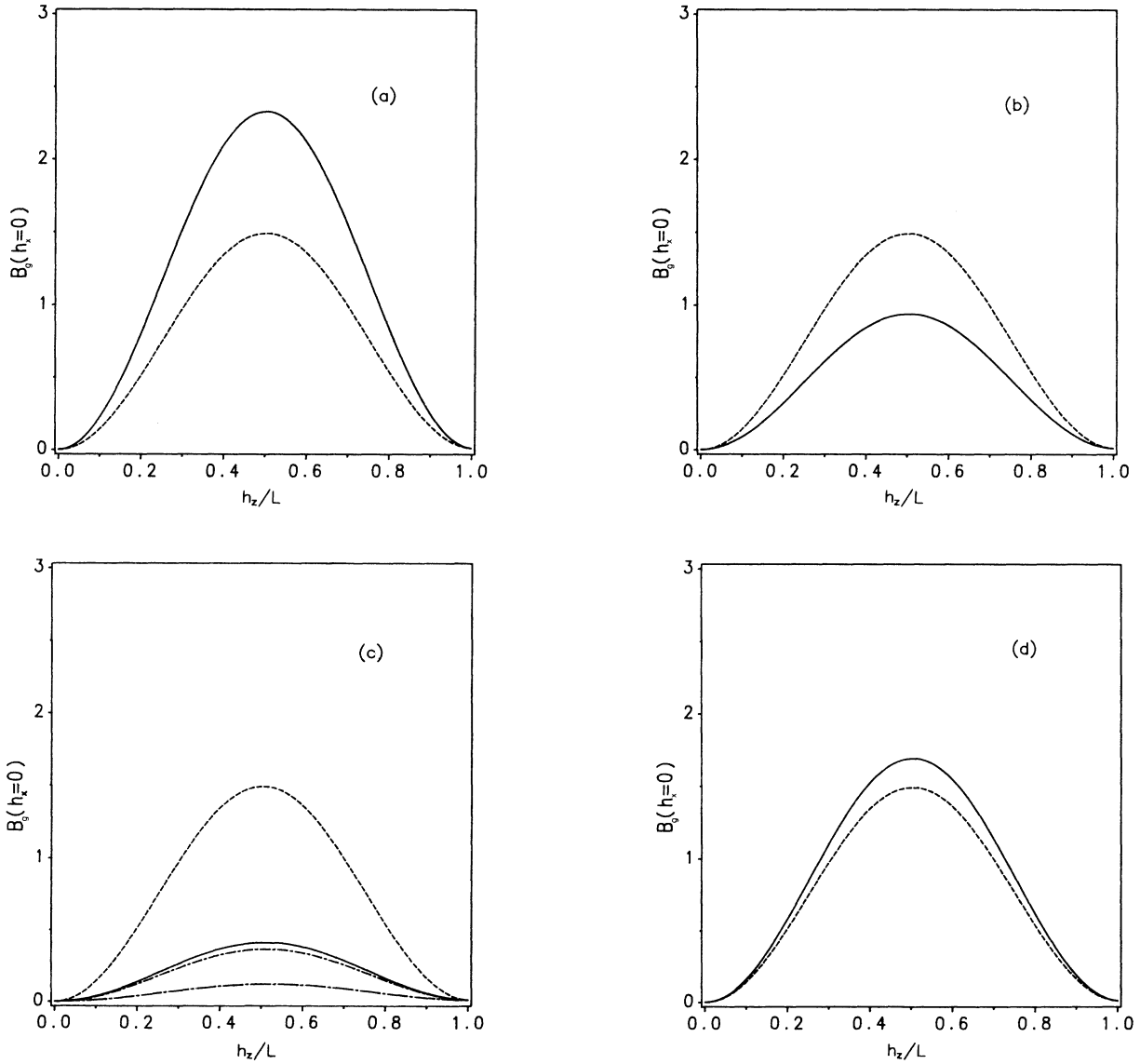

FIG. 8. $B_g(h_x=0)$ for $L=\lambda/2$, $R=0.99$, with $\theta_2=0.1$, $\delta=120$, $\eta=-\pi/2$, $N-M=-\frac{15}{32}$, and (a) $\xi=100$, (b) $\xi=150$, (c) $\xi=200$, with ideally matched result for $\theta_2=0.1$ (upper dot-dashed line) and $\theta_2=0.3$ (lower dot-dashed line), (d) $\xi=300$. The dashed line in each plot is the result obtained with no squeezed input.

$$\langle \beta_Y(k)\beta_Y(k')\rangle = -\frac{\hbar\mu_{21}^2K^3}{2\pi^2}M\frac{1+R}{1-R}\frac{1}{\mathcal{N}_g}\frac{\pi}{(1-R)^2}\mathrm{Re}[\mathcal{J}(\mathbf{h})^2]\delta(k+k')$$
$$+\frac{\hbar\mu_{21}^2K^3}{2\pi^2}N\frac{1+R}{1-R}\frac{1}{\mathcal{N}_g}\frac{\pi}{(1-R)^2}|\mathcal{J}(\mathbf{h})|^2\delta(k+k')$$
$$+\frac{\hbar\mu_{21}^2K^3}{4\pi^2}\frac{1+R}{1-R}\int_0^1 du(1+u^2)\frac{\sin^2(Kh_zu)}{1+F\sin^2(KLu)}\delta(k+k')$$
$$=\frac{\hbar\mu_{21}^2K^3}{6\pi^2}B_g(\mathbf{h})\delta(k+k')\ , \tag{4.26}$$

where

$$\mathcal{J}(\mathbf{h})=ie^{-i\eta}\int_{\cos\theta_2}^1 du(1+u)\sin^2(Kh_zu)J_0(Kh_x(1-u^2)^{1/2})\frac{1-R\cos(2KLu)-iR\sin(2KLu)}{1+F\sin^2(KLu)}$$
$$\times\exp[-(\delta+i\xi)(1-u^2)]\ . \tag{4.27}$$

Evidently, for maximum effect we require (i) that $\mathrm{Re}[\mathcal{J}(\mathbf{h})^2]$ be as close as possible to $|\mathcal{J}(\mathbf{h})|^2$, and (ii) that the factors multiplying N and M be maximized relative to the corresponding factor in the third term of (4.26) (i.e., the "normal" vacuum term).

Numerical results

In our first set of diagrams we display the results obtained with $L=\lambda/2$ and $R=0.99$, with $\theta_2=0.1$ rad. In Fig. 8 we give the profile of $B_g(\mathbf{h})$ at $h_x=0$ (where maximum reductions are to be expected), for a series of values of $\xi=100$, 150, 200, 300, with $\delta=120$ and $\eta=-\pi/2$ fixed. We assume an input squeezed by 94% ($N-M=-\frac{15}{32}$). In each case we plot the normal vacuum result as well (dashed line), and for the case $\xi=200$ we plot the result obtained with ideal matching as discussed previously (for $\theta_2=0.1$ and $\theta_2=0.3$). The magnitude of

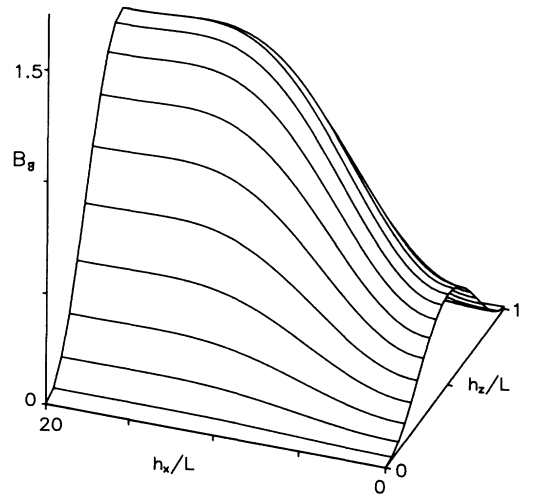

FIG. 9. B_g as a function of the x and y position coordinates, for $L=\lambda/2$, $R=0.99$, with $\theta_2=0.1$, $\delta=120$, $\xi=200$, $\eta=-\pi/2$, and $N-M=-\frac{15}{32}$.

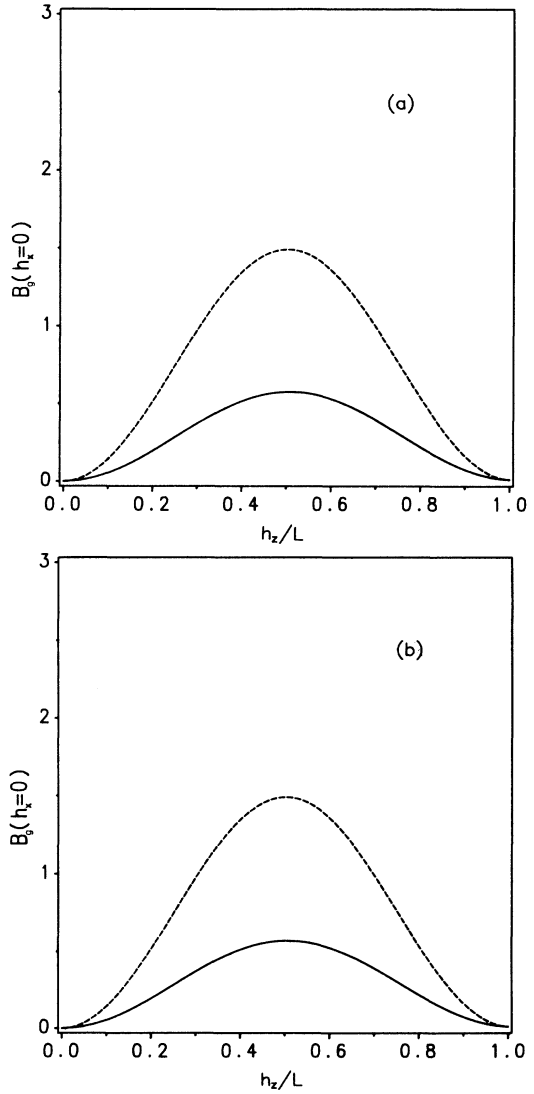

FIG. 10. $B_g(h_x=0)$ for $L=\lambda/2$, $R=0.99$, with $\theta_2=0.1$, $\xi=200$, $\eta=-\pi/2$, $N-M=-\frac{15}{32}$, and (a) $\delta=0$, (b) $\delta=300$. The dashed curve gives the normal vacuum result.

fluctuations relative to the vacuum depends strongly on the choice of ξ, emphasizing the need for good matching of the mode functions (in particular, the phase). Reduced fluctuations at $h_x=0$, are found for values of ξ in the range 130–290. At the position $h_z/L=0.5$, the optimum choice of parameters ($\delta\approx 120$, $\xi\approx 200$, $\eta=-\pi/2$) gives a maximum reduction below vacuum level of $\sim 72\%$. This compares very favorably with that obtained with ideal matching when $\theta_2=0.1$, but is somewhat less than the maximum possible reduction one could expect with an ideally matched input (with larger θ_2), as shown in Fig. 8(c).

In Fig. 9, we display the behavior in the x direction for the optimum choice of ξ and δ given above. This figure is to be compared with Fig. 2(b). Reduced values of B_g are found over a similar area to that when the input is ideally matched.

As we have seen, our results are very dependent on ξ. They are much less sensitive, however, to variations in δ, as we demonstrate in Fig. 10, where we fix $\xi=200$ and compare results for $\delta=0$ and 300. The graphs are virtually identical, and both give a maximum reduction below vacuum level of $\sim 60\%$ (the optimum choice of $\delta=120$ gives a 72% reduction).

Unlike the ideally matched case, increasing the angular limit θ_2 does not lead to an appreciable improvement in the amount of noise reduction possible. This is not surprising as the phase approximation used ceases to be effective for $\theta_k>0.1$, as shown in Fig. 7(b). If R is decreased slightly, then values of θ_2 larger than 0.1 give the best results (provided δ and ξ are fitted appropriately). However, a limit (above which no further improvement occurs) is again reached, with a maximum reduction in fluctuations similar to those found above. Our approximation to the phase is obviously limited, and some more accurate approximation would be needed to yield better reductions.

We shall not consider in detail any further approximations in this paper, but, in brief, Lorentzian approximations to the phase are found to give significant improvements over the above results, particularly as the angular limit θ_2 is increased. For example, if we replace $\eta+\xi\sin^2\theta_k$ by

$$-\frac{\pi}{2}\frac{w^2}{w^2+\theta_k^2}$$

in Eq. (4.24), then for $R=0.99$, $N-M=-\frac{15}{32}$, with $\theta_2=0.3$, one finds a reduction at $h_z/L=0.5$, $h_x/L=0$ of $\sim 88\%$ with the choice $w=0.057$, $\delta=90$. This is comparable to the result obtained with ideal matching, and exceeds the maximum reduction possible (for any θ_2) using a Gaussian distribution.

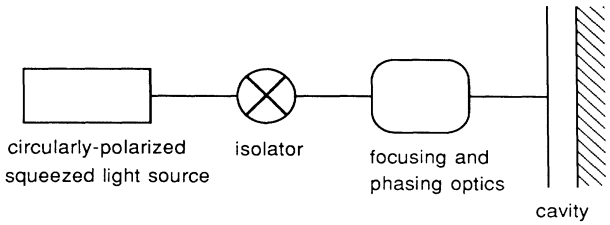

FIG. 11. Possible experimental setup.

V. EXPERIMENTAL CONSIDERATIONS

The experimental setup one might envisage is depicted in Fig. 11. As we have found, suitably prepared atoms inside the cavity will respond to only a single (circular) polarization of the field. Hence a single source of circularly polarized squeezed light should suffice.

This squeezed light would have to be passed through a system of lenses and phase plates in order to produce a focused beam of squeezed light with characteristics of the sort discussed earlier, that is, with appropriately matched phase and amplitude.

The cavity itself should be a bad cavity (i.e., low Q), which, in the case of a microscopic optical cavity, does not seem too difficult to achieve. In particular, we have, for the lifetime t_c of a photon within the cavity

$$t_c=\frac{L}{(1-R)c}\sim 10^{-13}\text{ s},$$

for $L\sim 10^{-6}$ m and $R=0.99$ (i.e., $Q\sim 100$). This time should be significantly shorter than the typical spontaneous-emission lifetime, so that the process can be regarded as irreversible. If this is not the case new effects may arise, such as the collective stimulated emission process observed by De Martini and Jacobovitz,[21] in which long-range atom-atom correlations occur when more than one atom undergoes a radiative decay within a period t_c. A low-density atomic or molecular sample would therefore also seem appropriate in avoiding such cooperative effects.

ACKNOWLEDGMENTS

We would like to thank Dr. R. E. Slusher for suggesting an investigation of microcavities, and Dr. M. J. Collett for some illuminating discussions. This work was partially financed by the New Zealand University Grants Committee.

[1]C. W. Gardiner, Phys. Rev. Lett. **56**, 1917 (1986).
[2]H. J. Carmichael, A. S. Lane, and D. F. Walls, Phys. Rev. Lett. **58**, 2539 (1987).
[3]H. Ritsch and P. Zoller, Opt. Commun. **64**, 523 (1987); S. An, M. Sargent, and D. F. Walls, *ibid.* **67**, 373 (1988).
[4]G. J. Milburn, Phys. Rev. A **34**, 4882 (1986).
[5]M. A. Marte and D. F. Walls, Phys. Rev. A **37**, 1235 (1988); M. A. Marte, H. Ritsch, and D. F. Walls, Phys. Rev. Lett. **61**,

1093 (1988).
[6]A. S. Parkins and C. W. Gardiner, Phys. Rev. A **40**, 2534 (1989).
[7]C. W. Gardiner, A. S. Parkins, and M. J. Collett, J. Opt. Soc. Am. B **4**, 1683 (1987); A. S. Parkins and C. W. Gardiner, Phys. Rev. A **37**, 3867 (1988); H. Ritsch and P. Zoller, Phys. Rev. Lett. **61**, 1097 (1988).
[8]F. De Martini, G. Innocenti, G. R. Jacobovitz, and P. Mataloni, Phys. Rev. Lett. **59**, 2955 (1987); F. De Martini and G. Innocenti, in *Quantum Optics IV*, edited by J. D. Harvey and D. F. Walls (Springer-Verlag, Berlin, 1986); see also W. Jhe, A. Anderson, E. A. Hinds, D. Meschede, L. Moi, and S. Haroche, Phys. Rev. Lett. **58**, 666 (1987), who use a microscopic plane-mirror cavity to demonstrate suppression of spontaneous decay at optical frequencies.
[9]C. W. Gardiner and M. J. Collett, Phys. Rev. A **31**, 3761 (1985).
[10]P. W. Milonni, Phys. Rep. **25**, 1 (1976).
[11]See, for example, the (one-dimensional) treatment of C. W. Gardiner and C. M. Savage, Opt. Commun. **50**, 173 (1984).
[12]M. Ley and R. Loudon, J. Mod. Opt. **34**, 227 (1987).
[13]C. K. Carniglia and L. Mandel, Phys. Rev. D **3**, 280 (1971).
[14]T. W. B. Kibble, in *Quantum Optics*, edited by S. M. Kay and A. Maitland (Academic, London, 1969).
[15]L. Allen and J. H. Eberly, *Optical Resonance and Two-Level Atoms* (Wiley, New York, 1975), Chap. 2.
[16]M. J. Collett and C. W. Gardiner, Phys. Rev. A **30**, 1386 (1984).
[17]L.-A. Wu, H. J. Kimble, J. L. Hall, and H. Wu, Phys. Rev. Lett. **57**, 2520 (1986); L.-A. Wu, M. Xiao, and H. J. Kimble, J. Opt. Soc. Am. B **4**, 1465 (1987).
[18]P. W. Milonni and P. L. Knight, Opt. Commun. **9**, 119 (1973); G. Barton, Proc. R. Soc. London, Ser. A **320**, 251 (1970).
[19]R. G. Hulet, E. S. Hilfer, and D. Kleppner, Phys. Rev. Lett. **55**, 2137 (1985).
[20]See, for example, A. Yariv, *Optical Electronics*, 3rd ed. (Holt, Rinehart and Winston, New York, 1985).
[21]F. De Martini and G. R. Jacobovitz, Phys. Rev. Lett. **60**, 1711 (1988).